International Journal of Modern Manufacturing Technologies
ISSN 2067–3604, Vol. XV, No. 2 / 2023
https://doi.org/ 10.54684/ijmmt.2023.15.2.7

AN APPROACH ON THE DESCRIPTION OF A FLAT DRIVING BELT BEHAVIOUR MIRRORED IN TRANSMITTED MECHANICAL POWER

Neculai-Eduard Bumbu, Mihaita Horodinca

”Gheorghe Asachi” Technical University of Iasi-Romania, Department of Digital Manufacturing Systems, Blvd. Mangeron, No. 41, 700050, Iasi, Romania

Corresponding author: Mihaita Horodinca, horodinca@tuiasi.ro

Abstract: For driving belt condition monitoring, the main interest is the certification of the capacity to keep their qualities unchanged over a long period of time and secondary to detect the imminence of the catastrophic failure. This paper presents a study on the behaviour detection and description of a flat driving belt health condition, used in a rotary machine electrically driven, particularly a lathe headstock gearbox running idle. It was discovered that in the mechanical power transmitted from electromotor to gearbox via a flat belt some specific sinusoidal components (a fundamental and some harmonics) of variable power are generated. The description of these power components (by values of amplitude, frequency and phase at origin of time) is indirectly detectable in the evolution of the active electrical power absorbed by the drive electromotor. Two arguments are available for this approach. Firstly, there is a reasonable assumption that between the mechanical power and the active electrical power there is an approximated proportionality relationship through the power efficiency. Secondly, the evolution of the active electrical power (or mechanical power as well) is a deterministic signal with a low level of noise. A simple computer assisted procedure of active electrical power signal acquisition and data processing was conceived, the detection was done by computer aided curve-fitting procedures in Matlab applied on active electrical power evolution absorbed by the driving motor in stationary working regimes (the electromotor playing the role of a mechanical power sensor). Mainly two ways of graphic representation have been proposed in order to describe the variable power generated by this flat belt (in time and frequency domains). The behaviour of many other types of belts involved in rotary machines driving can be similarly described.
Key words: Flat belt condition, monitoring, active electrical power, signal processing, curve fitting

1. INTRODUCTION

The power transmission systems through belts are still frequently used in actuated mechanical systems and rotary machines. The periodical checking of their properly working condition (especially the belts condition) is a matter of safety mainly helping to avoid the risks of breakdown. The health condition of many types of driving belts is an important topic addressed to monitoring and diagnosis. Relative frequently some shortcomings in operation related by belts integrity (wear, partial ruptures, tears, cracks, etc.) even before their failure affect the properly work of rotary machines. The detection of the end of properly operating life well in advance before a catastrophic breaking should be the minimum requirement of belts condition monitoring and diagnosis activities.
The optimal design and exploitation of a belt behaviour monitoring and diagnosis system requires a theoretical background focused mainly on the description of belt (and transmission) based on an appropriate dynamic model available at least in stationary (steady-state) working regimes condition. This model should consider some important issues as: the elastic properties of belts, their shape and materials, the belt-pulley friction contact phenomena, slippage and flexural vibrations, energy loss (belt transmission efficiency), belt tension etc. There are some consistent studies on this topic in the literature. Bucchi F. and Frendo F. [1] propose the validation of a model (as brush model) for the analysis of flat belts (mainly by finite element simulation) in steady-state working conditions. A comparison with other models was done (shear and creep model, Euler model etc.). The work of Dakel M., Jézéquel L. and Sortais J. L. [2] was involved in belt mechanics based on Eulerian description. They propose an analytical model of the pulley-belt system dynamics in stationary and transient regimes. Kim D., Leamy M. J. and Ferry A. A. [3] use the elastic/perfectly plastic friction law to define a flat belt drive nonlinear dynamic model during operation in steady-state regime. Scheidl J. [4] improve an existing mixed Eulerian-Lagrangian finite element model of two pulleys-belt drive taking into account the transverse deflections, gravity and frictional contact between pulleys and belt. Gao P. and Xie L. [5] performed a study on

static and dynamic characteristics of reliability models under the failure mode and slipping in order to estimate the failure rate. Pietra L. D., and Timpone F. [6] report some results related by belt tension research and their concordance with belt transmission theory and two models from literature (the Grashof's and Firbank's models). These models and their validation by experimental methods indicated the more important and convenient parameters involved in an appropriate description and condition monitoring of belts and belt transmissions, some of them already valued as the review paper of Zhu H., Zhu W. D. and Fan W. [7] reveals. Here, the failure analysis of power transmission belts is discussed, with a special approach dedicated on static and dynamic performance measurements (energy loss, vibrations, stress and strain, belt deformation etc.). The experimental evaluation of energy loss was also discussed. In [8] Krawiec P. *et al.* propose an approach on the energy losses in a flat belt transmission, some parameters being involved: torque capacity, slippage occurrence and belt transmission efficiency as a function of transmission load. The work of Fournier E. *et. al.* [9] was involved in a study of belt looseness inside a mechanical system (in steady-state regime) driven by an induction motor via a belt-pulley transmission.

A consistent part of previously researches reveals that, due to the dynamics of transmission, the evolution in time and frequency domains of some parameters are significantly useful in condition monitoring. Al Bulushi, A. A., Rameshkumar G. R. and Lokesha M. [10] proposes a methodology for condition monitoring of damaged belts based on vibration of the shafts where the pulleys are placed (revealed by accelerometers) described in time and frequency domains (by FFT). Ding H., Zhang Z. and Chen L. Q. [11] uses the amplitude spectrum of belt transverse vibration in order to highlight the possibilities to validate some resonant vibration reduction solutions and to confirm their analytical model. Hyun D., Kang T. J. and Kim J. propose in [12] to prevent the belt failure using an online condition detection method based on vibration monitoring (on acceleration spectrum). Pollak A. *et. al.* [13] proposes to use accelerometers and signal processing techniques in frequency domain in order to anticipate the flat belt failure. Yamashina H., Okumura S. and Kawai I. [14] propose a failure diagnose technique for V-belts based on power spectra of the vibration acquired at a driven bearing. The power spectra are calculated using a combination of cross-spectrum method (for noise reduction technique) and Bayes' discriminant function. Hu Y., *et. al.* [15] proposes a belt condition monitoring system based on an electrostatic sensor used to measure the speed and flexional vibrations. The spectrum analysis technique was used to detect and to describe the belt vibration modes and the relationship between their amplitude and belt speed. The work of Fehsenfeld M. *et. al.* [16] was focused on the influence of the belt tension on the transmission efficiency and the diminishment of breakdown risk. A fragmentation technique of the vibration signal in time domain was proposed in order to increase the confidence in the result of evolution in frequency domain. Fournier E. *et al.* [9] has studied also the effect of belt condition degradation, revealed in spectral signatures on spectra of some parameters related by driving motor (speed and phase current) or transmission behaviour (slip and vibration). Because the belt slippage is often the first symptom of belts breakdown, Brown R. E. [17] proposes an electronic system for continuous measurement of degree of slippage for a V-belt (by measuring the changes in belt transmission ratio).

It is expected that in the future there will be many other unexploited resources in experimental research of belt health condition, useful to improve or validate the theoretical approach or to increase the confidence in failure detection and prevention. This paper aims to present some new experimental facilities and results in computer assisted flat belt condition monitoring in time and frequency domains using the driving electric motor (a three phase asynchronous motor in this paper) as loading sensor. The evolutions of the electrical signals involved in description of electrical power absorbed by the motor (measured with a simple experimental setup) are available for computer assisted processing using some techniques (e. g. curve-fitting and fast Fourier transform). There is a simple reason for this approach: during a stationary operation regime of a machine-tool (e.g. a lathe headstock gearbox as rotary driven machine in this paper) the flat belt introduces a periodical variation of mechanical power, strictly related by belt pass frequency, which is firmly mirrored (and accurately described) in the variation of absorbed electrical power or its constituents (instantaneous power, current, power factor etc.). This description in electrical terms of the periodical mechanical power generated by flat belt (it depends mainly by belt condition and mechanical loading) is extracted from the entire signal using an adapted numerical signal extraction technique, acting as a multiple narrow band-pass notch filter. A simple experimental setup was built outside the computer for numerical sampling of the instantaneous current and voltage on a single electrical phase. Some of our previously published research results on a similar topic, especially related by mathematical description of instantaneous and active electrical power, current and instantaneous voltage are also available [18, 19].

The second section of this paper presents the experimental setup and some consideration on electrical parameters measurement, the third section is dedicated to results and discussion on experimental results, the fourth section presents the conclusion and future work.

2. MATERIALS AND METHODS

Figure 1 presents conceptually the experimental setup partially used already in [19]. A three-phase AC induction motor is used to drive a lathe headstock gearbox as rotary machine via a flat driving belt transmission (with a fabric flat belt, Figure 2). The drive pulley belt is placed on motor rotor on the input shaft of the gearbox, with kinematics described in [19]. The electrical power is supplied by a classical 50 Hz three-phase (A, B, C) network with a neutral wire N. Due to the evolution of mechanical loading the motor absorbs an electrical power measured through the values of instantaneous voltage $u(t)$ (as IV) and the absorbed instantaneous current $i(t)$ (as IC). A voltage transformer VT and a current transformer CT (Figure 1) placed on phase A are used to describe the evolution of IV and IC respectively (a reasonable assumption is that on all three phases the IV and IC is the same, except the phase shift $2\pi/3$). The IC and IV values are continuously acquired and converted in digital format (with the same sampling rate R) by a PCB USB oscilloscope PicoScope 4424 (from PicoTechnology, UK) and transferred to a computer for data processing using Matlab.

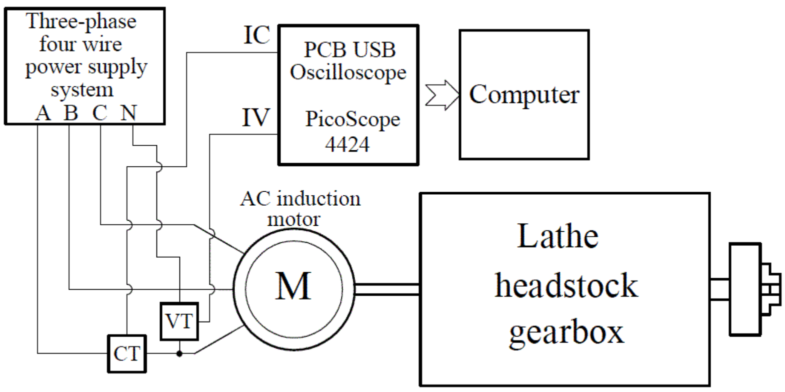

Fig. 1. A conceptual description of the monitoring system focused on the AC induction motor as loading sensor

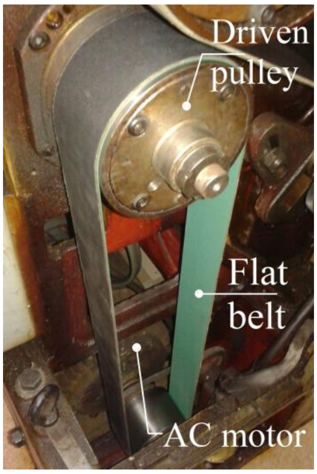

Fig. 2. The flat belt transmission

According with the definition, a numerical sample $u[t]$ of the IV value $u(t)$ and a numerical sample $i[t]$ of the IC value $i(t)$ define a sample $p[t]=u[t]\cdot i[t]$ of instantaneous electrical power (IEP). This IEP is the most significant electrical parameter involved in the description of mechanical loading and condition monitoring of parts inside the gearbox. It contains many type of information in frequency and time domain. For some reasons (e.g. because it is described with a big number of samples or because it contains high amplitude harmonics of 100 Hz as fundamental) sometime is replaced by active electrical power calculated as averaged IEP (as AEP_a) with a generic sample $P_a[t_m]$ on the m^{th} IEP period T_{IEP} (Eq. 1) or (as AEP_f) by IEP filtering with a moving average filter with n samples in the average, with a generic sample $P_f[t_l]$ Eq. 2). In both equation, n is the number of IEP samples on each period $T_{IEP}=1/100$ Hz, with $n\cdot\Delta t\approx T_{IEP}$, with $\Delta t = 1/R$ being the sampling time and R the sampling rate.

$$P_a[t_m] = \frac{1}{n}\sum_{k=nm}^{n(m+1)} p[t_k] \tag{1}$$

$$P_f[t_l] = \frac{1}{n}\sum_{i=1}^{n} p[t_{l-i}] \tag{2}$$

It is obvious that IV, IC, IEP and AEP_f have the same sampling rate R (as the number of samples on each second) and $R_a = R/n = 1/T_{IEP}$ is the sampling rate of AEP_a. The period T_{IEP} introduced above is the period of the dominant component of IEP having frequency f_{dIEP} =100 Hz (with $T_{IEP}=1/100$ s). There are $1/T_{IEP}$ samples per second of AEP_a. The time t_m from Eq. (1) is expressed as:

$$t_m = \left[\frac{n}{2}(2m+1)\cdot\Delta t\right] \tag{3}$$

The filter described in the definition of AEP_f from Eq. (2) works formally as a low-pass filter, it completely removes all the harmonics and the fundamental f_{dIEP}.

Figure 3 presents a view on the experimental evolutions of IC, IV (with conceptual descriptions as IC* and IV*), IEP and AEP_f (with real description) during a short sequence (60 ms) of stationary regime with the gearbox uncoupled (the motor drives only the flat belt transmission).
Here, IV* is a description of IV (with generic $k_v{\cdot}u[t]$ samples, as the numerical expression of the generic analog voltage $k_v{\cdot}u(t)$ delivered by the transformer VT) and IC* is a description of IC (with generic $k_c{\cdot}i[t]$ samples, as the numerical expression of the analog generic current $k_c{\cdot}i(t)$ delivered by the transformer CT). A sampling rate $R=25{,}000\ s^{-1}$ was used, with $n=250$ samples for each period T_{IEP}. Figure 4 describes a magnified evolution of AEP_f from Figure 3 (58 times on *y*-axis) and the evolution of AEP_a. As expected, there is a relative important variation of AEP_f mainly related by variable phenomena in flat belt transmission. The AEP_a evolution lost many details by comparison with AEP_f because of a R_a lower sampling rate (250 times smaller). Between each two samples of AEP_a a segment line is drawn. Even if the sampling rate of AEP_a is low ($R_a=100$ samples per second) it allows the valorisation of some important resources in the description of low frequency variable phenomena related by flat belt behaviour as proved below.

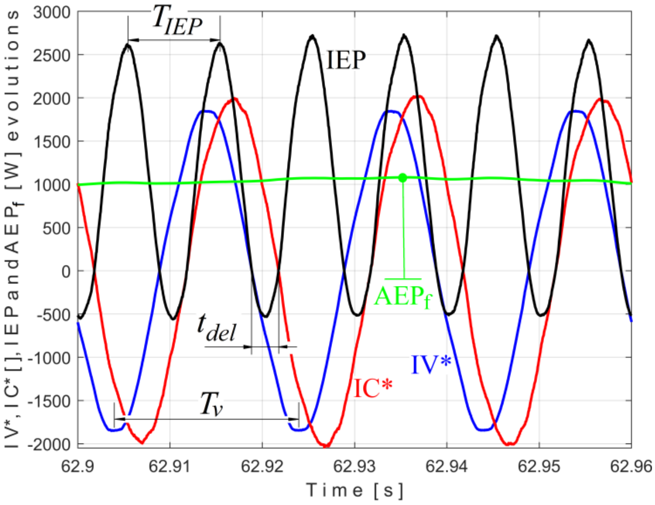

Fig. 3. A short sequence with IC*, IV*, IEP and AEP_f evolutions during a stationary regime (the motor drives only the flat belt transmission)

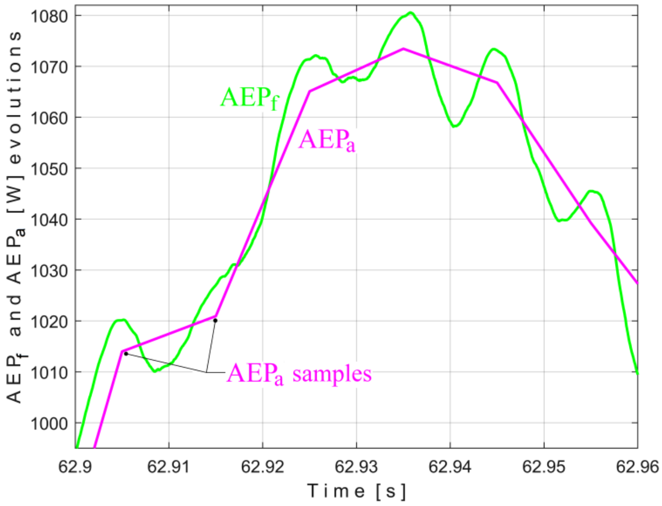

Fig. 4. The evolution of AEP_f from Figure 3 (with 58 times magnification on *y*-axis) and the evolution of AEP_a

The time delay t_{del} between zero-crossing moments of IV* and IC* (or IV and IC as well) is also an important item involved in the description of the active electrical power described as the IEP average on a period $T_v=1/50\ Hz$ (the period of IV*, Figure 3) calculated with integral function (as AEPi):

$$P_i[t_j] = \frac{1}{T_v}\int_{t=jT_v}^{T_v(j+1)} p(t)\,dt = U_{RMSj}\cdot I_{RMSj}\cdot cos(\varphi_j) \tag{4}$$

Here, U_{RMSj} and I_{RMSj} are the root mean square values (RMS) of the IV and IC (theoretically the amplitude of IV or IC divided by square root of 2) on the period *j*, the time t_j is defined as $t_j=jT_v+T_v/2$. There are 50 samples P_i on each second. A generic time delay t_{delj} describes a generic power factor $cos(\varphi_j)$ as:

$$cos[\varphi_j] = \cos\left(2\pi\cdot\frac{t_{delj}}{T_v}\right) \tag{5}$$

The variation of AEP_i is strictly related by the variation of I_{RMSj} and the variation of PF, reasonably assuming that U_{RMSj} is constant (a hypothesis partially contradicted in [18]). The working regimes of motors with negative active power absorption are characterized by a negative value of PF (the RMS of current being permanently positive). There are available 100 samples of PF on each second. It is interesting to remark that with $T_v=2T_{IEP}$, Eq. (1) is a numerical approximation of Eq. (4) if $n{\cdot}\Delta t\approx 2T_{IEP}$.
There is an important hypothesis related by monitoring resources offered by IV, IC, IEP, AEP_a, AEP_f and PF in lathe headstock gearbox monitoring (already confirmed before in [19]): these are deterministic signals, their variable part can be described mainly as a sum of sinusoidal components (at least on short periods of time) mixed with some low amplitude non-deterministic components (including noise). As example, for AEP_a evolution in stationary regime it is available the description below:

$$P_a[t_m] = \bar{P} + [\sum_{i=1}^{h} P_{Ai} \cdot \sin(2 \cdot \pi \cdot f_i \cdot t_m + \alpha_i)] + P_{ndc}[t_m] \quad (6)$$

Here $\bar{P}$ is the average value of AEP$_a$, P_{ndc} is the non-deterministic and not describable part of AEP$_a$, due to the fact that the numerical description should respect the Nyquist frequency f_{Nq}: with h established so that the upper limit of f_i (as f_h) is f_{Nq}. This Nyquist frequency is half of the sampling rate (for AEP$_a$ $f_{Nq}=50\ Hz$)
As previously was proved in [19], this paper claims that some sinusoidal components from Eq. (6) are generated by the flat belt. The determination of the description of the sinusoidal components related by flat belt behaviour (in other words the finding out the values of amplitude P_{Ai}, frequency f_i and phase α_i at origin of time for some components involved in Eq. (6)) during the stationary regime previously considered (only the flat belt transmission is driven by motor) is the main challenge of this work. Two signal processing techniques are used: the amplitude spectra generated with fast Fourier transform (FFT) and curve-fitting procedure, both in Matlab.

3. RESULTS AND DISCUSIONS

In Figure 5 a short sequence with $N_s=500$ samples of AEP$_a$ evolution (with $R_a=100$ samples per second during 5 s) of this stationary regime is depicted. The average value $\bar{P}$ (1009 W) and a 50 Hz component electrically generated (with 44.087 W amplitude and 0.7264 rad as phase at origin of time) was mathematically removed, in the left side of Eq. (6) remains an AEP$_a$ written as $P_a^*[t_m] = P_a[t_m] - \bar{P}$.

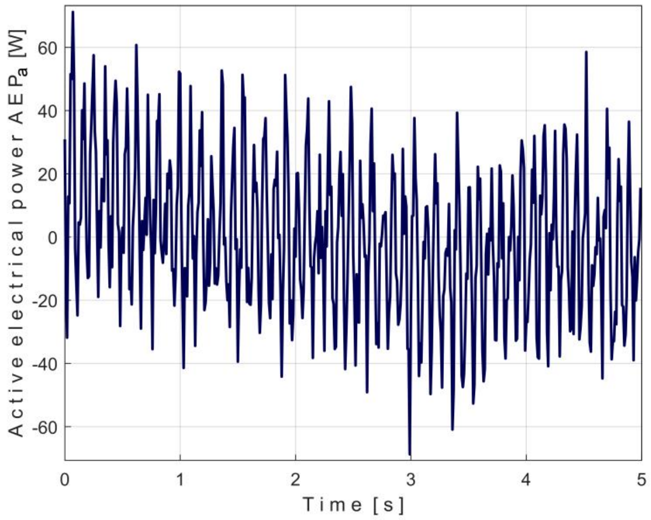

Fig. 5. A short sequence (5 s) with AEP$_a$ ($P_a^*[t_m]$) evolution during a stationary regime (only the flat belt transmission is driven)

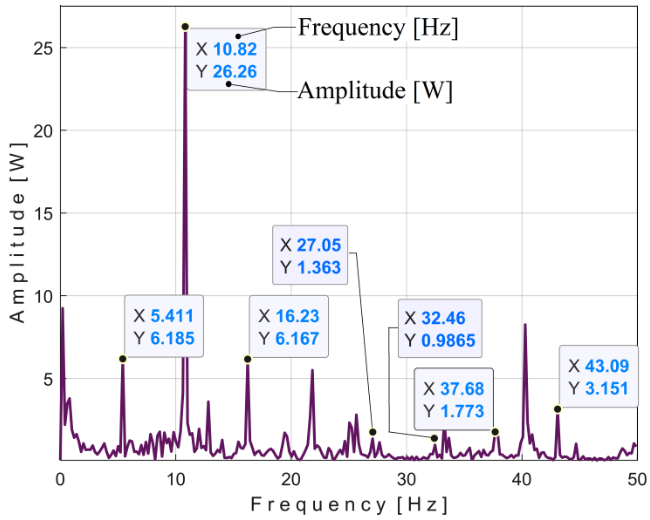

Fig. 6. The FFT amplitude spectrum of the AEP$_a$ evolution from Figure 5

In figure 6 the FFT amplitude spectrum of the sequence from Figure 5 (until the Nyquist limit) is depicted. Because a low number of samples ($N_s=500$) the frequency resolution in spectrum (f_{rs}) is low, being defined as $f_{rs}=R_a/N_s=0.2\ Hz$.
There is a first argument that the major part of this AEP$_a$ signal is deterministic: the occurrence of many big distinct peaks, each one describing the amplitude and the frequency of a significant sinusoidal component inside AEP$_a$ and described by a label which indicates the frequency and the amplitude. It is important to underline that the labelled components from Figure 6 are generated by the flat belt, an issue discussed later on.
Unfortunately, this FFT spectrum doesn't provides the values of phases at origin of time, this being an impediment in monitoring (apart from other disadvantages, e. g. the low frequency resolution in spectrum). That is why the curve-fitting procedure is privileged in this study, the FFT amplitude spectrum being used from now only for confirmation. There are two ways for finding the signal components description in AEP$_a$ by curve-fitting: the use of curve-fitting application from Matlab or to use an own written program for this purpose. This last option is privileged in this work. Basically, the description of sinusoidal components in AEP$_a$ is found one by one, starting by the components with biggest amplitude. A reasonable large range and a reasonably big number of values in each range are established for amplitude (generically labelled P_{Acfj}), frequency (generically labelled f_{cfj}) and phase (generically labelled α_{cfj}) at origin of time for each component j. These values are automatically and systematically changed by computer in each range until are found those optimal values (P_{Acfj}^r, f_{cfj}^r and α_{cfj}^r) which produce a minimum in the difference written below:

$$\sum_{m=1}^{N_s} \left| P_a^*[t_m] - P_{Acfj}^r \cdot \sin(2 \cdot \pi \cdot f_{cfj}^r \cdot t_m + \alpha_{cfj}^r) \right| \rightarrow min \tag{7}$$

This curve-fitting strategy is repeated few times successively, every time by reducing each of three ranges (for amplitude, frequency and phase at origin of time) around the previously determined optimal values (P_{Acfj}^r, f_{cfj}^r and α_{cfj}^r) until Eq. (7) produces the lowest minimum acceptable value.

If (as hypothesis) $P_a^*[t_m]$ contains only h sinusoidal components, with $f_h < f_{Nq}$ (in other words, in Eq. (6) $P_{ndc}\,[t_m] = 0$ whatever the value of m it is) and a perfect description of all these components inside $P_a^*[t_m]$ is found by curve fitting, then the result depicted below is produced:

$$\sum_{m=1}^{N_s} \left| P_a^*[t_m] - \sum_{j=1}^{h} P_{Acfj}^r \cdot \sin(2 \cdot \pi \cdot f_{cfj}^r \cdot t_m + \alpha_{cfj}^r) \right| = 0 \tag{8}$$

As example, a first result using this curve-fitting procedure is related by the finding-out the description of sinusoidal component with biggest amplitude in the spectrum from Figure 6, described as:

$$f(t_m)=27.32875 \cdot \sin(2 \cdot \pi \cdot 10.7757 \cdot t_m + 3.3999) \tag{9}$$

In Figure 7 is drawn the evolution described by Eq. (9) overlapped on the evolution of $P_a^*[t_m]$ depicted in Figure 5. Figure 8 presents a zoomed-in detail of Figure 7.

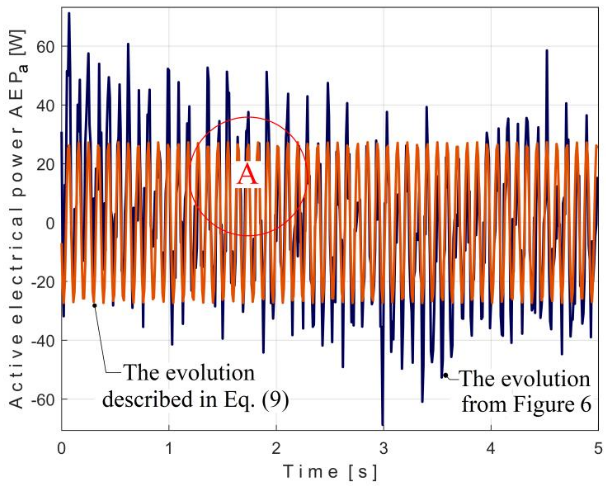

Fig. 7. The AEP$_a$ ($P_a^*[t_m]$) evolution from Figure 5 and the graphical description of Eq. (9) with first curve-fitting result (the dominant component from Figure 6)

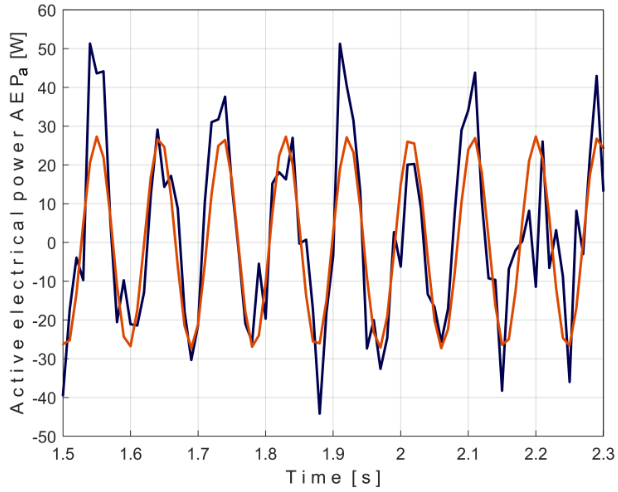

Fig. 8. A zoomed-in detail in area A of Figure 7

These discontinuous (fragmented) evolutions are due to a low sampling time of AEP_a description ($R_a = 100\ s^{-1}$, $\Delta t = 0.01\ s$). It is evident that there is a relative good fit (the best accepted by fitting criteria) between both evolutions. The accuracy of fitting is better described by the FFT amplitude spectrum of the residual from Figure 9. This residual is mathematically described with Eq. (10).

$$R_1 = P_a^*[t_m] - 27.32875 \cdot \sin(2 \cdot \pi \cdot 10.7757 \cdot t_m + 3.3999) \tag{10}$$

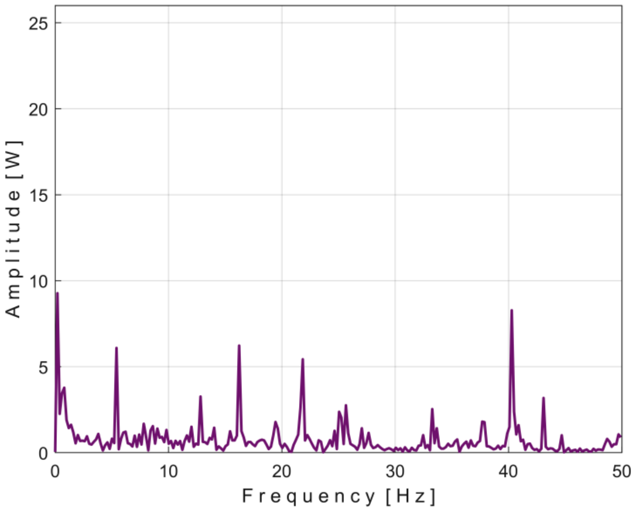

Fig. 9. The amplitude FFT spectrum of the residual from Eq. (10) or of $P_a^*[t_m]$ from Figure 5 after the mathematical subtraction of the dominant sinusoidal component depicted in Eq. (9) as well

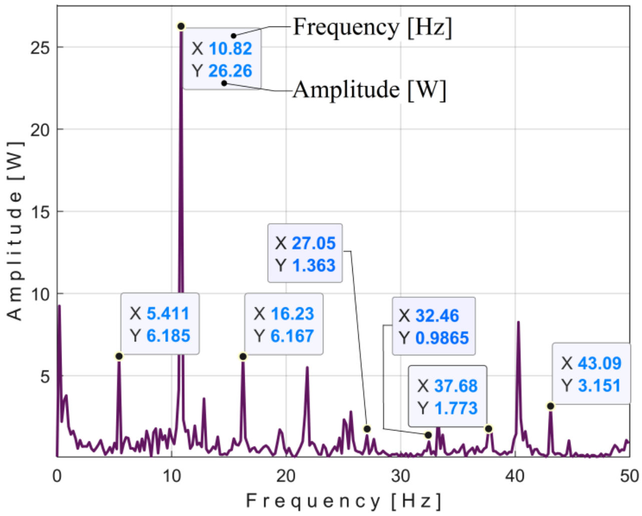

Fig. 10. The amplitude FFT spectrum of the $P_a^*[t_m]$ from Figure 5. A copy of Figure 6

The accuracy of this first curve fitting result is obvious: by comparison between Figures 9 and 10 (this being a copy of Figure 6). This dominant peak in spectrum totally disappears. In the same way it is possible to find out and to describe the major part of the sinusoidal components from $P_a^*[t_m]$. A total number of h=*44* sinusoidal components were found. The result of subtraction of these components from $P_a^*[t_m]$ defines a residual graphically depicted in red on Figure 11 (drawn over $P_a^*[t_m]$ evolution from Figure 5). The accuracy of the description of these components is clearly indicated, firstly by the peak to peak variation of the residual (35.77 W), evidently smaller compared with peak to peak variation of $P_a^*[t_m]$ (139.9 W).

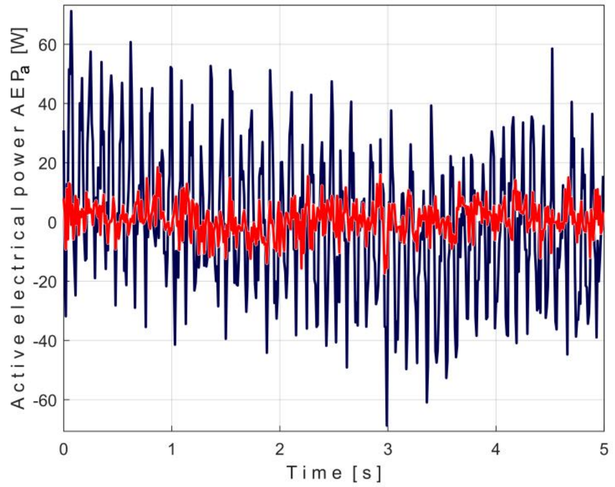

Fig. 11. The AEP_a ($P_a^*[t_m]$) evolution from Figure 5 and the graphical description of residual (in red) after mathematical subtraction of 44 sinusoidal components found by curve-fitting

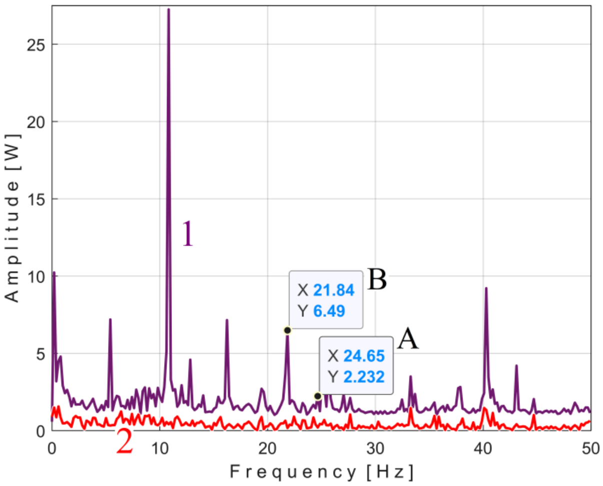

Fig. 12. The FFT amplitude spectrum of the $P_a^*[t_m]$ from Figure 6 (curve 1, moved up with 0.5 W) compared with the FFT amplitude spectrum of the residual from Figure 11 (curve 2, in red)

There is a second argument for the accuracy of the description of these 44 sinusoidal components, the FFT amplitude spectrum of the residual compared with the FFT amplitude spectrum of $P_a^*[t_m]$, as depicted in Figure 12. There is a strong amplitude reduction of all peaks. For sure, some peaks have not been completely removed; this means that the resources of curve fitting procedure were not fully valorised.

Now an important question arises: there are some sinusoidal components in AEP$_a$ ($P_a^*[t_m]$) evolution generated by the flat belt?

Among the $h=44$ sinusoidal components found by curve-fitting there are two, depicted by the labels A and B on Figure 12. Because the spectrum was moved up with 0.5 W, for graphical reasons, both amplitudes should be diminished by 0.5 W. The frequency of component A (having a more accurate value determined by curve-fitting as $f_A=24.559$ Hz) is exactly the motor rotor rotation frequency where the drive pulley ($d_A=121$ mm diameter) of the flat belt transmission is placed (Figure 2). The frequency of component B (having a more accurate value determined by curve-fitting as $f_B=21.806$ Hz) is exactly the rotation frequency of the input shaft in the gearbox, where the driven pulley ($d_B=139$ mm diameter) is placed. The transmission ratio related by diameters $(d_B+g)/(d_A+g)=1.146$ (here g being the thickness of the belt) is very close by the transmission ratio related by frequencies $f_A/f_B=1.126$. Two reasons explain the difference: first, the slippage in the transmission; second, the variation of rotation speed of the motor (the curve-fitting procedure supposes that this speed is constant). The length of the flat belt being $L_{fb}=1800$ mm, the belt pass frequency f_{bp} can be calculated as $f_{bp} = f_B \cdot \pi (d_B+g)/L_{fb}=5.366$ Hz. This is very close by the frequency of the first labelled peak (5.411 Hz) from Figure 6 (or 10 as well), more accurately described by curve-fitting with the frequency of 5.399 Hz. As Figure 6 (or 10 as well) clearly indicates by labels, this sinusoidal component (acting as a fundamental component F_{bs}) has six other sinusoidal components H_{bsi} as harmonics of this belt pass frequency having (with a good approximation) the frequencies of $f_{bpsHi}=(i+1)\cdot f_{bps}$. A completely description of these seven components generated by the flat belt found on FFT spectrum and by curve fitting is described in left side of Table 1.

Here, for the components found on FFT amplitude spectra P_{bs} and P_{bsi} describe the amplitudes, f_{bps} and f_{bpsHi} describe the frequencies. Here for the components found by curve-fitting P_{bc} and P_{bci} describe the amplitudes, f_{bpc} and f_{bpcHi} describe the frequencies and φ_{bpc} and φ_{bpci} describe the phases at origin of time.

Table 1. Two descriptions of the sinusoidal components generated by the flat belt

	Found on FFT amplitude spectra (Figure 6)			Found by curve fitting		
Component	Amplitude [W]	Frequency [Hz]	Phase at origin of time [rad]	Amplitude [W]	Frequency [Hz]	Phase at origin of time [rad]
F_b	$P_{bs}=6.185$	$f_{bps} = 5.411$	Not available	$P_{bc}=6.074$	$f_{bpc} = 5.390$	$\varphi_{bpc} =6.132$
H_{b1}	$P_{bs1}=26.26$	$f_{bpsH1} =10.82$	Not available	$P_{bc1}=27.328$	$f_{bpcH1} =10.775=1.999\, f_{bpc}$	$\varphi_{bpc1} =3.399$
H_{b2}	$P_{bs2}=6.167$	$f_{bpsH2} =16.23$	Not available	$P_{bc2}=6.688$	$f_{bpcH2} =16.168=2.999\, f_{bcp}$	$\varphi_{bpc2}=1.807$
H_{b3}	Unavailable (hidden by the peak B from Figure 12)			$P_{bc3}=2.006$	$f_{bpcH3} =21.537=3.995\, f_{bpc}$	$\varphi_{bpc3} =4.869$
H_{b4}	$P_{bs4}=1.363$	$f_{bpsH4} =27.05$	Not available	$P_{bc4}=1.526$	$f_{bpcH4} =26.935=4.997\, f_{bpc}$	$\varphi_{bpc4} =2.006$
H_{b5}	$P_{bs5}=0.986$	$f_{bpsH5} =32.46$	Not available	$P_{bc5}=0.680$	$f_{bpcH5} =32.399=6.010\, f_{bpc}$	$\varphi_{bpc5} =5.971$
H_{b6}	$P_{bs6}=1.773$	$f_{bpsH6} =37.68$	Not available	$P_{bc6}=2.653$	$f_{bpcH6} =37.723=6.998\, f_{bpc}$	$\varphi_{bpc6} =6.006$
H_{b7}	$P_{bs7}=3.151$	$f_{bpsH7} =43.09$	Not available	$P_{bc7}=2.792$	$f_{bpcH7} =43.012=7.979\, f_{bpc}$	$\varphi_{bpc7} =6.704$
H_{b8}	Unavailable			$P_{bc8}=0.880$	$f_{bpcH8} =48.490=8.996\, f_{bpc}$	$\varphi_{bpc8}=3.981$

It is obviously that the curve fitting is a more convenient procedure to detect and to describe the sinusoidal components, firstly- because it provides the values of phases at origin of time, secondly- because the description of amplitudes, frequencies and phases is more accurate.

A new question arises: why these components related by the flat belt occur and how their amplitudes are related by belt condition?

The flat belt works as an elastic body with (ideally) constant stiffness along its length. If we suppose that the driven shaft in belt transmission introduces a constant mechanical loading (viscous and dry friction) no reason to have variation of mechanical power (and AEP$_a$ as well) generated by belt. If, on contrary, for some reasons, this stiffness is not constant on the full length of the belt (locally smaller as normal, due to a manufacturing error, a local tear or crack etc.) the circulation of the belt over its pulleys generates a periodical variation of transmitted mechanical power, having the same frequency with belt pass frequency f_{bp}. This is simple to explain: for a complete belt movement cycle, when the small stiffness region is placed on the tight side of the belt, the transmitted mechanical power decreases, when the part with normal stiffness is placed on the same tight side, the transmitted mechanical power increases. This periodical variation of transmitted mechanical power is responsible for the occurrence of the harmonically correlated sinusoidal components F_b and H_{bi} already revealed and described before in Table 1.

The description of these components provided by curve-fitting (with the results available in the right side of Table 1) allows in a first approach the opportunity to establish the evolution in a appropriate range of time domain of the variable mechanical power generated by the flat belt (via its imagine AEP$_a$ labelled as P_b), based by mathematical description from below:

$$P_b(t) = P_{bc} \cdot \sin(2 \cdot \pi \cdot f_{bpc} \cdot t + \varphi_{bpc}) + \sum_{i=1}^{8} P_{bci} \cdot \sin(2 \cdot \pi \cdot f_{bpci} \cdot t + \varphi_{bpci}) \quad (11)$$

A reasonable assumption is that between mechanical power and AEP_a there is proportionality through the inverse of power efficiency (involved in the transformation from electrical to mechanical power inside the motor).

In order to increase the availability of this result for belt condition monitoring there is a second approach (as frequency correlation) in the description above: all the frequencies are very slightly adjusted in order to have a strictly harmonic correlation with the fundamental (the frequency of i^{th} harmonic should be exactly $i+1$ times the frequency of the fundamental). The frequency f_{bpc} of the fundamental is renamed f_{bpch} and recalculated as:

$$f_{bpch} = \frac{1}{9}\left(f_{bpc} + \sum_{i=1}^{8} \frac{1}{i+1} f_{bpcHi}\right) \quad (12)$$

Based on values of frequencies f_{bpc} and f_{bpcHi} from Table 1, Eq. (12) defines the value $f_{bpch}=5.387\ Hz$, very close by $f_{bpc}=5.390\ Hz$. Based on result from Eq. (12) the description from Eq. (11) is:

$$P_{bh}(t) = P_{bc} \cdot \sin(2 \cdot \pi \cdot f_{bpch} \cdot t + \varphi_{bpc}) + \sum_{i=1}^{8} P_{bci} \cdot \sin[2 \cdot \pi \cdot f_{bpch}(i+1) \cdot t + \varphi_{bpci}] \quad (13)$$

There is a second approach (as the changing of the origin of time). It supposes that the origin of time ($t=0$) for $P_{bh}(t)$ is moved with t_0, at the first positive zero-crossing moment (from negative to positive values) of the fundamental, with t_0 in relationship with φ_{bpc} and the frequency f_{bpch} as:

$$2\pi \frac{t_0}{T_{bpch}} = 2\pi \cdot t_0 \cdot f_{bpch} = \varphi_{bpc} \text{ whence it follows } t_0 = \frac{\varphi_{bpc}}{2\pi \cdot f_{bpch}} \quad (14)$$

In Eq. (14) $T_{bpch}=1/f_{bpch}$ is the period of the fundamental. Due to this second approach, $P_{bh}(t)$ is depicted as $P_{bh0}(t)$ and in the right side of Eq. (13) t is replaced with t-t_0, with t_0 from Eq. (14) as follows:

$$P_{bh0}(t) = P_{bc} \cdot \sin\left[2 \cdot \pi \cdot f_{bpch} \cdot \left(t - \frac{\varphi_{bpc}}{2\pi \cdot f_{bpch}}\right) + \varphi_{bpc}\right] + \\ + \sum_{i=1}^{8} P_{bci} \cdot \sin[2 \cdot \pi \cdot f_{bpch}(i+1) \cdot (t - \frac{\varphi_{bpc}}{2\pi \cdot f_{bpch}}) + \varphi_{bpci}] \quad (15)$$

Eq. (15) can be rewritten after simplification in a simpler shape, as:

$$P_{bh0}(t) = P_{bc} \cdot \sin[2 \cdot \pi \cdot f_{bpch} \cdot t] + \sum_{i=1}^{8} P_{bci} \cdot \sin[2 \cdot \pi \cdot f_{bpch}(i+1) \cdot t + \varphi_{bpci} - (i+1) \cdot \varphi_{bpc}] \quad (16)$$

By comparison with Eq. (15), in Eq. (16) the angle φ_{bpc} disappears while the phase φ_{bpci} at origin of time are changed and being recalculated as φ_{bpci} - $(i+1) \cdot \varphi_{bpc}$.

A graphical representation of the variable power $P_{bh0}(t)$ from Eq. (16) generated by the flat belt during a sequence of 1 s with the same sampling rate with AEP_a (100 samples per second or 100 s^{-1}) is done (as $P_{bh01}(t)$) in Figure 13 (curve 1). Curve 2 depicts the evolution of the fundamental. As previously discussed, the origin of time for both curves is a positive zero-crossing moment of the fundamental. A better description of $P_{bh01}(t)$) is done if the sampling rate is increased 10 times, at 1,000 s^{-1}, as Figure 14 indicates.

The evolution of $P_{bh01}(t)$) from Figure 13 can be expressed in frequency domain- as Figure 15 presents- by FFT amplitude spectra. As expected, the spectrum is not well defined (especially related by amplitudes) because of a low number of samples, the frequency resolution in spectrum is low (1 Hz). A better result is obtained if the simulation from Figure 13 is extended at 10 s, using 1000 samples. The FFT amplitude spectrum in these conditions (now with the frequency resolution of 0.1Hz) is depicted in Figure 16, with a zoomed-in detail having an upper limit at 7.5W (for a better description of low amplitude peaks).

The results from Table 1, the reconstruction of $P_{bh01}(t)$ evolution in time domain (Figure 14) and the spectrum of this reconstruction from Figure 16, (despite its inaccuracy) are important results in flat belt condition monitoring.

A significant feature of this belt behaviour is related by relatively high amplitude of the first harmonic (H_{b1}). A first (experimentally unconfirmed) hypothesis states that on the entire belt there are two equidistant areas with low stiffness (e. g. two cracks). A second hypothesis states that the dynamic system of the rotor inside the motor has a vibration mode close by the f_{bpsH1} frequency. This excited vibration mode generates a resonant amplification, consequently the increasing of amplitude of this first harmonic. This second hypothesis was experimentally confirmed: when the entire gearbox is driven by flat belt transmission this amplitude decreases significantly due to the increasing of damping (dry and viscous friction generated inside the gearbox).

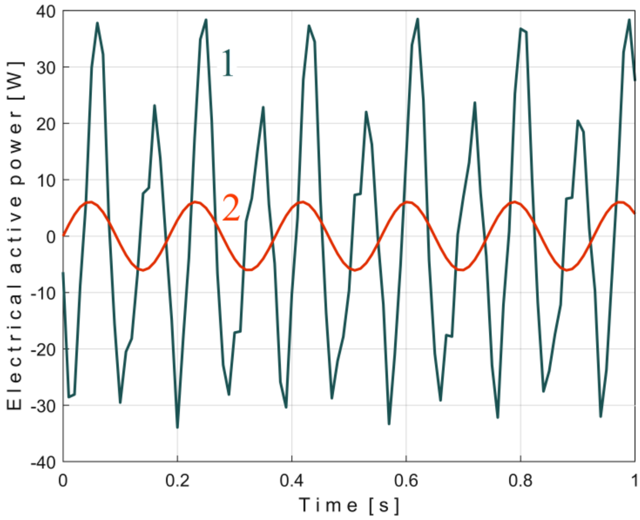

Fig. 13. Curve 1: the evolution of variable mechanical power generated by the flat belt mirrored in AEP$_a$ $P_{bh01}(t)$ during 1 s (sampling rate 100 s^{-1} and 100 samples). Curve 2: the evolution of the fundamental

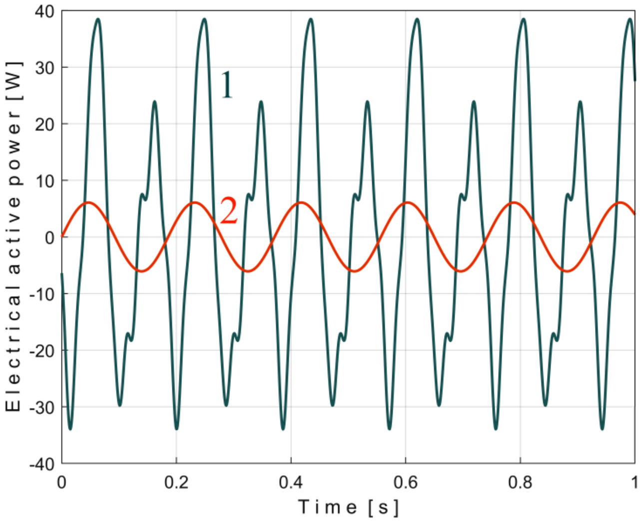

Fig. 14. The evolutions from Figure 13 drawn with 1000 s^{-1} sampling rate (1000 samples)

There is a simple way to increase and to confirm the reliability of this approach in flat belt condition monitoring: a new sequence of $P_a^*[t_m]$ similarly with that described in Figure 5 was acquired (but after 95 seconds of continuously running of the flat belt transmission) and processed in both way (by FFT and by curve fitting) as before. Table 2 presents the results of this processing (only by curve fitting).

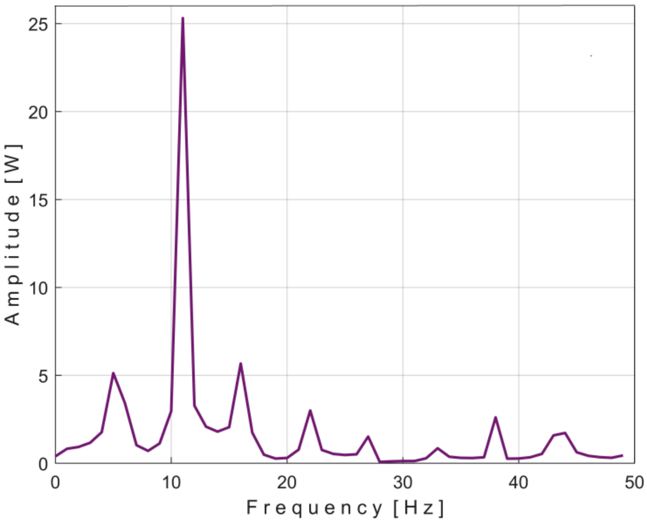

Fig. 15. The FFT amplitude spectrum of $P_{bh01}(t)$ from Figure 13 (100 samples the sampling rate 100 s^{-1}, during 10 s)

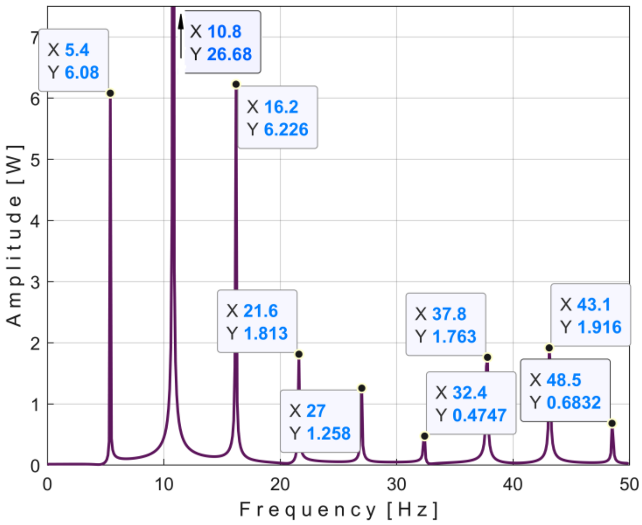

Fig. 16. The FFT amplitude spectra of a sequence of $P_{bh01}(t)$ with 1000 samples (the sampling rate 100 s^{-1}, during 10 s)

Based on the results from Table 2, similarly with Figure 14, Figure 17 describes a reconstruction of a $P_{bh0}(t)$ evolution (as $P_{bh02}(t)$) also during 1 second, using a sampling rate of 1000 s^{-1} (with 1000 samples). There are strong similitudes between Figures 17 and 14, better highlighted in Figure 18, where both evolutions are overlapped.

Table 2. The description of the sinusoidal components generated by the flat belt, found by curve-fitting in a new $P_a^*[t_m]$ sequence, 95 seconds later

	Found by curve fitting		
Component	Amplitude [W]	Frequency [Hz]	Phase at origin of time [rad]
F_b	$P_{bc}= 6.756$	$f_{bpc} = 5.380$	$\varphi_{bpc} =3.569$
H_{b1}	$P_{bc1}=25.413$	$f_{bpcH1} =10.773=2.002\, f_{bpc}$	$\varphi_{bpc1} =4.722$
H_{b2}	$P_{bc2}=5.905$	$f_{bpcH2} =16.152=3.002\, f_{bcp}$	$\varphi_{bpc2}=0.777$
H_{b3}	$P_{bc3}=3.128$	$f_{bpcH3} =21.576=4.010\, f_{bpc}$	$\varphi_{bpc3} =6.487$
H_{b4}	$P_{bc4}=1.322$	$f_{bpcH4} =26.963=5.011\, f_{bpc}$	$\varphi_{bpc4} =2.108$
H_{b5}	$P_{bc5}=0.870$	$f_{bpcH5} =32.255=5.995\, f_{bpc}$	$\varphi_{bpc5} =0.425$
H_{b6}	$P_{bc6}=2.532$	$f_{bpcH6} =37.691=7.005\, f_{bpc}$	$\varphi_{bpc6} =1.816$
H_{b7}	$P_{bc7}=2.583$	$f_{bpcH7} =43.015=7.995\, f_{bpc}$	$\varphi_{bpc7} =4.342$
H_{b8}	$P_{bc8}=0.850$	$f_{bpcH8} =48.468=9.008\, f_{bpc}$	$\varphi_{bpc8}=0.974$

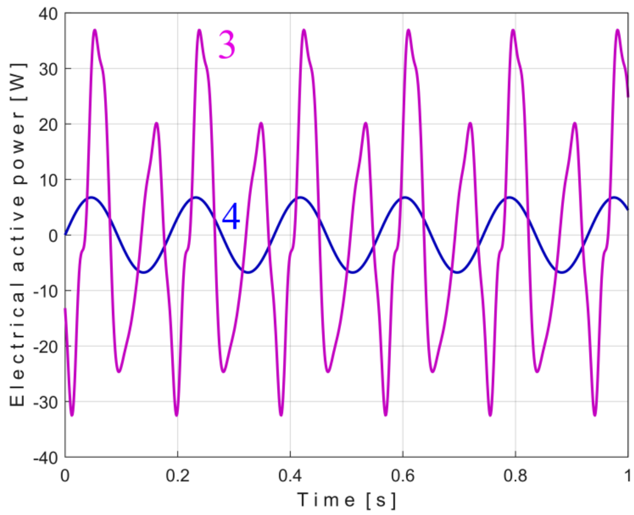

Fig. 17. A reconstruction (3) of $P_{bh02}(t)$ and the fundamental (4) detected inside a new sequence $P_a^*[t_m]$ of AEP$_a$ evolution 95 s later

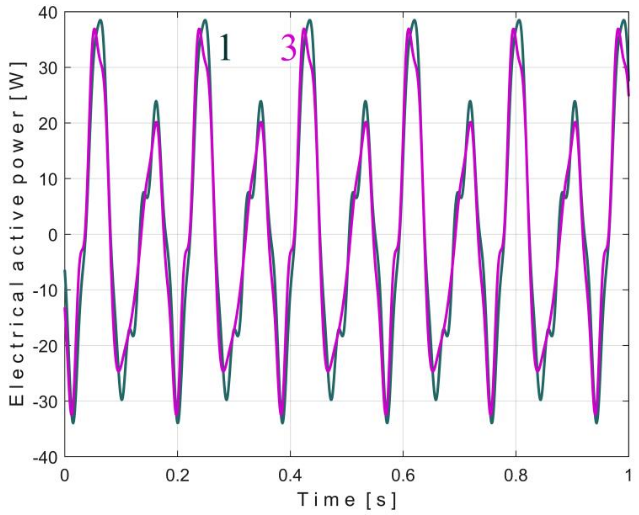

Fig. 18. An overlapping of $P_{bh01}(t)$ evolutions (1 from Figure 14) and $P_{bh02}(t)$ evolution (3 from Figure 17).

This overlapping is possible because both graphical evolutions ($P_{bh01}(t)$ and $P_{bh02}(t)$) have a strictly harmonic correlation with the fundamental (according with discussion above, Eq. (12)) and because each evolution has the same origin of time in a positive zero-crossing moment of it fundamental (according with discussions above, Eq. (14), (15) and (16)).

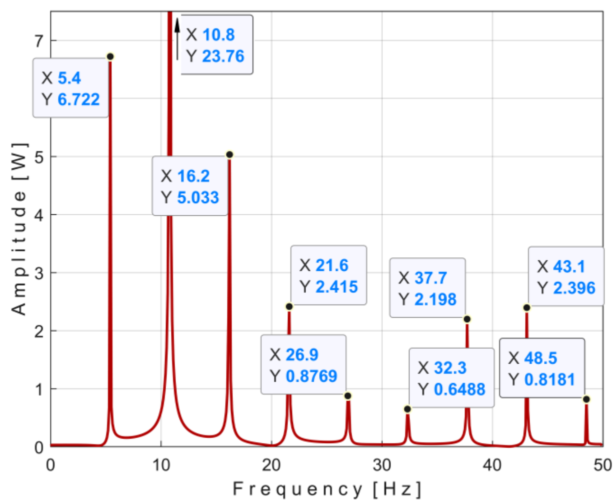

Fig. 19. The FFT amplitude spectra of a sequence of $P_{bh02}(t)$ with 1000 samples (the sampling rate 100 s^{-1}, during 10 s)

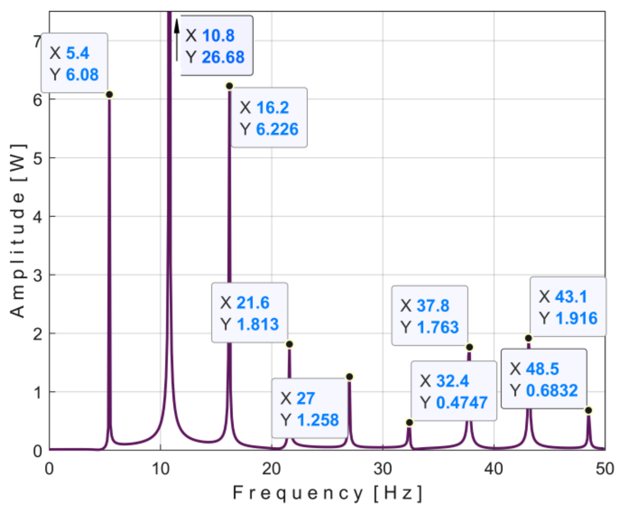

Fig. 20. The FFT amplitude spectra of a sequence of $P_{bh01}(t)$ with 1000 samples (the sampling rate 100 s^{-1}, during 10 s). A copy of Figure 16

The similarities of these evolutions from Figure 18 strongly increases the confidence in this approach of monitoring, the evolution of $P_{bh0}(t)$ (here particularly as $P_{bh01}(t)$ and $P_{bh02}(t)$) in time domain is a feasible characterisation of this flat belt health condition. The differences between these evolutions characterize the normal changing of belt condition probably related by the temperature (due the heating generated by flat belt transmission). We should mention that (at least) the visual inspection of the flat belt we use did not reveals any structural defect associated with local rupture or cracking, probably the only reason for this variation of this $P_{bh0}(t)$ power is the local variation of belt stiffness due to some (allowable) manufacturing errors.
The evolution in time domain of this second reconstruction $P_{bh02}(t)$ from Figure 17 can be also depicted in frequency domain (by FFT amplitude spectrum, similarly with Figure 16), as Figure 19 indicates.
By comparison, Figure 20 presents a copy of the spectrum (of $P_{bh01}(t)$) from Figure 16. The overlapping of spectra is not relevant here. As expected there are completely similarities between spectra related by the frequencies of the components, and relatively small differences between amplitudes, another argument for the feasibility of this approach.
Some supplementary experimental research studies reveal that the $P_{bh0}(t)$ evolution in time and frequency produces relevant results in many other stationary regimes (with an increasing of average power transmitted by belt). Some other types of belts (at least the V-belts) produce in the same conditions similar results.

4. CONCLUSIONS

The novelty of this study is a new approach in flat belt health condition monitoring, mainly based on an appropriate computer assisted signal processing technique (by curve-fitting) of the active electrical power (as AEP_a with 100 s^{-1} sampling rate) absorbed by the drive motor of the belt transmission in stationary regimes.
A simple experimental setup based on a three phase AC induction motor which drives a lathe headstock gearbox through a flat belt transmission was used. A voltage transformer and a current transformer placed on a phase of the electrical supply system provides a description of the instantaneous voltage and current delivered to the motor, numerical acquired by computer, used to describe the absorbed AEP_a.
Due to manufacturing errors (variation of stiffness in this study) or usually due to a malfunction (e. g. local ruptures, tires and cracks, etc.) the belt generates a periodical variation of mechanical power (with belt pass frequency) firmly mirrored in the evolution of AEP_a absorbed by the motor. This variation is mainly related by the belt health condition. The periodical variation of AEP_a generates by the flat belt contains sinusoidal components with a fundamental (having the belt pass frequency) and some harmonics. The mathematical description of each of these sinusoidal components (through the values of amplitudes, frequencies and phases at origin of time) was found using a curve-fitting procedure made with an own program in Matlab. Based on these descriptions the variable part of AEP_a generated by the flat belt was built using a higher sampling rate (1000^{-1}). The mathematical shape of this AEP_a (as a sum of sine) was adapted in order to accomplish two criteria: a strictly harmonic correlation of components (with a slightly changing of frequencies) and to have the origin of phase in a positive zero-crossing of the fundamental. This way is possible to compare in time domain the evolution of variable AEP_a generated by the flat belt in different working conditions, as briefly was exemplified in this paper on an undamaged belt. Two experimental results confirm each other the availability of this approach.
The main purpose of this paper was mainly to introduce this new approach in belt condition monitoring. A future approach intends to improve the depth of research, e. g. by identifying how different types of belt structural defects are described in the AEP_a evolution, particularly those due to deterioration as a result of normal and heavy operation. The resources of power factor, instantaneous current and voltage will be also used in a future work.

REFERENCES

1. Yamashina, H., Okumura, S., Kawai, I., (1996). *Development of a diagnosis technique for failures of V-belts by a cross-spectrum method and a discriminant function approach*, J. Intell. Manuf., 7(1), 85-93.
2. Zhu, H., Zhu, W. D., Fan, W., (2021). *Dynamic modeling, simulation and experiment of power transmission belt drives: A systematic review*, J. Sound Vib., 491, 11579.
3. Kim, D., Leamy, M. J., Ferri, A.A., (2011). *Dynamic Modeling and Stability Analysis of Flat Belt Drives Using an Elastic/Perfectly Plastic Friction Law*, J. Dyn. Syst.-T. ASME, 133, 041009-1.
4. Krawiec, P., Warguła, Ł., Walu´s, K. J., Gawronska, E., Ságová, Z., Matijošius, J., (2022). *Efficiency and Slippage in Draw Gears with Flat Belts*, Energies, 15, 9184.
5. Al Bulushi, A. A., Rameshkumar, G. R., Lokesha, M., (2015). *Fault Diagnosis in Belts using Time and Frequency based Signal Processing Techniques*, Int. J. Multidisc. Sci. Eng., 6(11), 12-20.
6. Hyun D., Kang T. J., Kim J., (2021). *Fault Diagnosis of Belt Driving Power Transfer Facility Using*

Vibration Analysis, J. Electr. Eng. Technol., 16, 2257-2264.
7. Dakel, M., Jézéquel, L., Sortais, J. L., (2018). *Stationary and transient analyses of a pulley-belt system based on an Eulerian approach*, Mech. Mach. Theory, 128, 682-707.
8. Bucchi, F., Frendo, F., (2022). *Validation of the brush model for the analysis of flat belt transmissions in steady-state conditions by finite element simulation*, Mech. Mach. Theory, 167, 104556.
9. Scheidl, J., (2020). *Motion of a friction belt drive at mixed kinematic description, International Journal of Solids and Structures*, Int. J. Solids Struct., 200-201, 158-169.
10. Pollak, A., Temich, S., Ptasinski,W., Kucharczyk, J., Gasiorek, D., (2021). *Prediction of Belt Drive Faults in Case of Predictive Maintenance in Industry 4.0 Platform*, Appl. Sci., 11, 10307.
11. Gao P., Xie, L., (2017). Reliability models of belt drive systems under slipping failure mode, Adv. Mech. Eng., 9(1), 1–10.
12. Pietra, L. D., Timpone, F., (2013). *Tension in a flat belt transmission: Experimental investigation* , Mech. Mach. Theory, 70, (129-156).
13. Ding, H., Zhang, Z., Chen, L. Q., (2018). *Vibration Reduction Effect of One-Way Clutch on Belt-Drive Systems*, Eur. J. Mech. A-Solid, 71, 378-385.
14. Yamashina, H., Okumura, S., Kawai I., (1996). *Development of a Diagnosis Technique for Failures of V-Belts by a Cross-Spectrum Method and a Discriminant Function Approach*, J. Intell. Manuf., 7, 85-93.
15. Feksenfeld, M., Kuhn, J., Wielitzka, M., Ortmaier, T., (2020). *Tension Monitoring of Toothed Belt Drives Using Interval-Based Spectral Features*, IFAC Papersonline, 53(2), 728-743.
16. Fournier, E., Picot, A., Regnier, J., Andrieux, C., Saint-Michel, J., Maussion, P., (2015). *Effects of Transmission Belt Looseness on Electrical and Mechanical Measurements of an Induction Motor*, Proceedings of 10th International Symposiumon Diagnostics for Electrical Machines, Power Electronics and Drives (SDEMPED), pp. 259-265, Portugal (Guarda).
17. Brown, R. E., (2012). *The development of an electronic system to continually monitor, indicate and control, 'belt slippage' in industrial friction 'V' belt drive transmission systems*, J. Phys. Conf. Ser., 364, 012055
18. Bumbu, N. E., Horodinca, M, (2022). *The Mirroring of a Transient Regime of a Lathe Headstock Gearbox in the Evolution of Supplying Voltage of the AC Driving Motor*, Recent, 23(1), 20-30.
19. Horodinca, M., Bumbu, N.E., Chitariu, D. F., Munteanu, A., Dumitras, C.D., Negoescu, F., Mihai, C. G., (2023). *On the Behaviour of an AC Induction Motor as Sensor for Condition Monitoring of Driven Rotary Machines*, Sensors, 23(1), 488.

Received: April 16, 2023 / Accepted: December 15, 2023 / Paper available online: December 20, 2023 © International Journal of Modern Manufacturing Technologies